01 Feb 2023

Effect of Additional Water or Superplasticizer on Key Characteristics of Cement Paste Made with Superabsorbent Polymer and Other Shrinkage Mitigating Materials

Kamran Aghaee

Ricarda Sposito

Karl Christian Thienel

Kamal Khayat
Missouri University of Science and Technology, khayatk@mst.edu

Recommended Citation

K. Aghaee et al., "Effect of Additional Water or Superplasticizer on Key Characteristics of Cement Paste Made with Superabsorbent Polymer and Other Shrinkage Mitigating Materials," *Cement and Concrete Composites*, vol. 136, article no. 104893, Elsevier, Feb 2023.
The definitive version is available at https://doi.org/10.1016/j.cemconcomp.2022.104893

Cement and Concrete Composites 136 (2023) 104893

Contents lists available at ScienceDirect

Cement and Concrete Composites

journal homepage: www.elsevier.com/locate/cemconcomp

Effect of additional water or superplasticizer on key characteristics of cement paste made with superabsorbent polymer and other shrinkage mitigating materials

Kamran Aghaee [a], Ricarda Sposito [a,b], Karl-Christian Thienel [b], Kamal H. Khayat [a,*]

[a] Department of Civil, Architectural and Environmental Engineering, Missouri University of Science and Technology, 500 W 16th Street, Rolla, MO, 65409, USA
[b] Institute for Construction Materials, University of the Bundeswehr Munich, Werner-Heisenberg-Weg 39, 85579, Neubiberg, Germany

ARTICLE INFO

Keywords:
Expansive agent
Internal curing
Microstructure
Shrinkage
Shrinkage reducing admixture
Superabsorbent polymer

ABSTRACT

The use of superabsorbent polymer (SAP) coupled with expansive agent (EA) or shrinkage-reducing admixture (SRA) can effectively reduce shrinkage of cement-based materials. However, SAP particles at high contents can adversely affect rheological and mechanical properties. Securing proper workability can be accomplished by additional water or adjusting the superplasticizer (SP) demand. There is an uncertainty about the efficiency of these approaches to workability compensation. This study evaluates the effect of additional water or SP on key properties of cement paste made with SAP and relatively high content of EA or SRA. Macro and micro mechanisms underlying the effect of combined shrinkage mitigating strategies on the performance of cement paste made with 0.4 water-cementitious materials ratio are investigated. Results indicate higher efficiency of increasing SP demand by 0.6% versus the addition of water by 30 g per gram of SAP. Up to 80% higher compressive strength is obtained for the mixtures made with additional SP, which is attributed to up to 33% reduction in capillary porosity and smaller pore-size distribution of the hydrated cement paste. In the presence of high EA content, the use of additional SP prevents excessive initial expansion in the paste with additional water.

1. Introduction

Autogenous shrinkage refers to the macroscopic deformation of paste in a closed and isothermal condition due to the development of hydrostatic tensile stresses in capillary pores. Once the autogenous shrinkage exceeds the threshold tensile stress of the concrete, especially at early ages, microcracks form that increase the transport mechanisms and drop the durability of concrete [1,2]. Autogenous shrinkage is particularly critical in concrete with high binder content and low water-cementitious materials ratio (w/cm), such as high-strength concrete and ultra-high performance concrete [3]. The use of shrinkage-mitigating materials, such as expansive agent (EA), shrinkage-reducing admixture (SRA), and internal curing (IC) using superabsorbent polymer (SAP) or pre-saturated lightweight aggregate (LWA) can mitigate autogenous and drying shrinkage and reduce the risk of cracking [4–6].

EAs, which compensate for shrinkage with initial expansion are commonly classified into calcium sulfoaluminate (CSA-), CaO-, and MgO-based EA. The former requires huge amounts of water for the formation of ettringite. In addition, the hydration products resulting from CSA-based EA can be unstable and can cause delayed ettringite formation, which increases the risk of cracking at later ages [7]. Therefore, the other types of EA are preferred [8,9]. The CaO-based and MgO-based EAs form mainly $Ca(OH)_2$ and $Mg(OH)_2$, respectively, with significantly lower water demand. The hydration of CaO-based EA can lead to an expansion of up to 90% in the presence of adequate amount of water [10]. The presence of sufficient water is essential for the hydration of both cement and EA when they are used together. Otherwise, at low water to cementitious ratio (w/cm) there would be the possibility of lack of water for the hydration of cement grains due to the high water absorption by EA [11]. Zhao et al. [12] reported higher water demand and shorter dormant period by incorporating 2 wt% CaO-based EA in cement paste proportioned with w/cm of 0.35 compared to the reference paste without EA. The reason for this feature was quick occurrence of the maximum level of Ca^{2+} concentration in the presence of EA.

The reactivity of MgO-based EA is controlled by the MgO calcination temperature, where a higher temperature slows down the reaction kinetics [13]. As observed by Wang et al. [13], the addition of MgO- or CaO-based EA led to a higher hydration rate, and the CaO-based EA was

* Corresponding author.
E-mail address: kkhayat@mst.edu (K.H. Khayat).

https://doi.org/10.1016/j.cemconcomp.2022.104893
Received 21 September 2022; Received in revised form 19 November 2022; Accepted 8 December 2022
Available online 13 December 2022
0958-9465/

more effective even at lower content and humidity. The heat release using 3 wt% CaO-based EA was 20% higher than 6 wt% MgO-based EA, after 7 days. The use of 3% CaO-based EA reduced the 28-day autogenous shrinkage of the ultra-high performance concrete (UHPC) by 70% in comparison with 6% MgO-based EA, which reduced the shrinkage by only 24%.

SRAs are organic surfactant chemicals including mono-alcohols with a hydroxyl function group, glycols, polyoxyalkylene glycol alkyl ethers, polymeric surfactants, and amino alcohols which are able to reduce both autogenous and drying shrinkage [14]. In the water-solvent medium of concrete, the surfactant molecules, due to their amphipathic nature, are adsorbed to the non-polar interfaces, such as water-air, water-oil, and water-solid interfaces. By the electrostatic attraction, the surfactant's polar head is adsorbed to the nonpolar tail in the pore solution of concrete and decreases its surface tension. This stems from the electrostatic repulsion between the polar heads of the adjacent surfactant molecules [15]. In addition to the effective shrinkage reduction by SRA, its adverse effect on mechanical properties, hydration, and pore structures of concrete has been reported extensively [16–20]. For example, Lopes et al. [21] used up to 2 wt% SRA in high strength concrete (C80) mixtures with w/cm of 0.3. The authors reported that the use of SRA slightly increased the slump and significantly reduced the autogenous shrinkage of concrete. The initial compressive strength was significantly reduced, while only a 5% drop in 28-day compressive strength was reported. This was associated with the effect of SRA on initial hydration by declining the dissolution of alkalis in the pore solution and slowing down the hydration hereby. The mercury intrusion porosimetry test results indicated higher total porosity and change in pore size distribution, which led to higher gel porosity and formation of mesopores using 2 wt% SRA.

SAPs are commonly composed of cross-linked and acrylate-based network structures with acryl amide or acrylic acid namely monomers beside the main chains [22,23]. When evenly distributed in the cement matrix, SAPs can rapidly absorb some of the mixing water that can be released slowly into the cement matrix during cement hydration [24]. This reduces the risk of self-desiccation, shrinkage and crack formation [24–26]. Although SAPs are effective in reducing shrinkage, their absorption/desorption kinetics are highly dependent on its physical and chemical characteristics [27–29]. De Meyst et al. [30] reported that the use of 0.25 wt% SAP with particle size of 100 μm was more effective than 40 μm in shrinkage mitigation of cement paste with w/cm of 0.35, especially at initial ages. This was justified by smaller surface to volume ratio of the coarser SAP and its prompt internal curing (IC) water release, versus the less active surface zone of the finer SAP and potential filling and blockage of particles with hydration products [30,31]. In addition to shrinkage reduction, an accelerating effect on the hydration was reported by the use of SAP in cement paste with w/cm of 0.36 and UHPC with w/cm of 0.2 [32,33], where the authors explained the acceleration by a higher alkalinity of the matrix resulting from a more concentrated pore solution. An enhanced formation of portlandite was observed by Esteves et al. [34] and by Justs et al. [35], especially in the pores stemming from swollen SAP after water desorption. Contrary to this, Zhao et al. [12] found that the addition of 0.15 wt% and 0.30 wt% SAP prolonged the dormant period by up to 0.8 h due to the absorption of water. These SAP contents also significantly extended the deceleration period, indicating a slower dissolution of C_3A. Li et al. [36] found that the incorporation of SAP prolonged the dormant period by up to 2 h and led to a later and up to 30% lower main peak of alkali-activated slags at different w/cm. The authors explained it by the absorption of Ca^{2+} and Al^{3+} stemming from slag by SAP and their gradual release into pore solution to reach thresholds of Ca/Si and Al/Si required to form C-A-S-H. The chemical structure of SAP plays a significant role in its internal curing performance and shrinkage mitigation. Zhong et al. [6] utilized SAPs with different chemical structures and found that SAPs with high density of anionic functional groups accelerated the absorption of pore solution and desorption due to the anionic groups and multivalent cations complexing in the pore solution. SAPs with low density of anionic groups exhibited significantly lower adsorption. SAPs with either non-ionic groups or both anionic and cationic groups did not release the absorbed solution. Higher molar ratio of acrylic acid/sodium acrylate in SAP network resulted in higher desorption. Although all the selected SAP types were effective in mitigating autogenous shrinkage, SAPs with anionic functional groups induced rapid expansion on the first day, due to quick desorption, followed by slower expansion afterwards. Zhu et al. [37] studied the chemical and physical characteristics of SAP composed of poly (sodium acrylate-acrylamide) copolymer with varying concentrations of poly sodium acrylate on its swelling and mechanical properties in different ionic solutions containing Na^{+}, Ca^{2+}, and Al^{3+}. A strong relationship between the type of ions in the solution and swelling of the SAP was reported; the highest swelling ratio was obtained by the solution containing Na^{+} in both low and high concentrations of poly sodium acrylate. It was observed that the presence of Ca^{2+} and Al^{3+} in the absorbed solution can considerably reduce the SAP swelling capacity. The Al^{3+} created a mechanically stiff barrier layer on the SAP surface, which prevented the desorption and increased the overall elastic modulus of the SAP from 10 kPa to 100 kPa compared to Ca^{2+} solutions.

Several researchers used SAP with additional water, and although zero autogenous shrinkage was observed, an adverse effect on pore structure, strength, setting time, and rheological properties was reported [32,33,38–40]. The reason for this degradation was the increased microporosity, as a result of swollen SAP particles [32,39,41]. However, other researchers indicated the positive effect of SAP with additional water on the performance of concrete [41–43]. For example, Geiker et al. [44] used 0.4 wt% SAP by maximum diameter of 250 μm in mortar mixtures (w/cm = 0.35). The authors reported 20% higher compressive strength at 28 days due to the higher internal relative humidity and degree of hydration.

The combination of shrinkage mitigating materials has shown to be very effective in eliminating shrinkage. For example, Valipour and Khayat [45] found that the coupled effect of 60 vol% saturated lightweight sand with CaO-based EA, MgO-based EA or SRA could reduce the autogenous shrinkage by up to 600 μm/m at 91 days, compared to 495 μm/m when the saturated lightweight sand was used alone. There is evidence that the combination of shrinkage mitigating materials at reasonable contents can reduce the impairing effect of their individual use at high content. The combination of EA and SRA significantly mitigated autogenous shrinkage and resulted in a reasonable expansion after 28 days [46]. In addition, the coupled system led to slightly higher compressive strength compared to the individual use of EA/SRA. A multi-objective optimization based on rheological, mechanical and autogenous shrinkage properties revealed that the combinations of 10 wt% EA with either 0.125 wt% SAP or 1 wt% SRA are the most effective combinations in producing cement paste with high strength, flowability, and thixotropy and without autogenous shrinkage [46].

The reduction of workability due to the use of SAP can be adjusted by using an additional water content or superplasticizer (SP) dosage rate. However, limited work is available on the combination of extra water and SP or only SP. For example Adams et al. [47] used 0.2 wt% SAP in mortar with 0.42 w/cm and compared the effect of using additional water and SP on mortar performance. The results showed that the additional water and SP (effective w/cm of 0.49 and 0.52) resulted in sharper compressive and flexural strength development. The authors reported microstructural refinement and absence of microcracks of the mixtures made with SAP and lower w/cm of 0.42. The review of previous studies reveals the significant lack of knowledge regarding the use of SAP with additional SP to compensate for workability loss instead of using additional water in the presence of high content of other shrinkage mitigating materials. The current study elucidates the effect of SAP in the presence of 10 wt% EA or 2 wt% SRA on macro mechanical properties and microstructure development of the cement paste mixtures. The mechanism of the workability compensation approaches on compressive strength, autogenous shrinkage, and microstructural characteristics of cement paste made with SAP coupled with EA or SRA is

elaborated.

2. Materials and methods

2.1. Materials

An ordinary Portland cement (OPC), Type I/II conforming to ASTM C150-22, was used in this study. A CaO-based EA was employed to compensate for autogenous shrinkage by the initial expansion due to the hydration of CaO. Table 1 provides the chemical composition, including the loss on ignition (LOI), and the Blaine specific surface area as provided by the supplier.

A non-ionic angular covalently cross-linked acrylamide SAP with a median particle size of 52.4 μm was used to provide IC and improve autogenous shrinkage. The particle size distribution of powder materials is shown in Fig. 1a. The molecular weight of the SAP (Mc value) between the cross-links was 1.3×10^5 g/mol. Its maximum water absorption and desorption rate in filtered solution with w/cm of 5:1, were 30 g/g and 95 wt%, respectively (Fig. 1b). The mass of SAP employed to compensate for early-age shrinkage was determined using Eq. (1) [5].

$$M_{SAP} = \frac{C_f \, CS \, \alpha_{max}}{S \, W_{SAP}} \quad (1)$$

where, M_{SAP} is the mass of dry SAP (kg/m^3), C_f is the cement content (kg/m^3), CS is the early age shrinkage of cement including chemical and autogenous shrinkage. According to the previous studies conducted by the authors [46,48], CS of 0.15 was applied to eliminate early age shrinkage. α_{max} is the maximum expected degree of hydration (1), S is the absorption rate of SAP in filtrated pore solution, and W_{SAP} is the SAP desorption rate upon equilibrium 95% relative humidity, which is expressed as a fraction of oven-dry mass.

A polycarboxylate-based SP at 0.2%-0.8 wt% was used to secure adequate flowability. SRA was utilized to reduce shrinkage by decreasing the surface tension of the capillary pores. The solid content and the specific gravity of SRA and SP are given in Table 2. The liquid part of SRA (70 wt%) was considered and deducted from the mixing water.

2.2. Mixing and curing

In total, seven cement paste mixtures (Table 3) were prepared with a constant w/cm of 0.4. In the mixtures prepared with SAP, the rapid water absorption by the SAP was compensated for in two ways, namely by adding extra water (30 g H_2O/g SAP) and by adjusting the SP dosage to secure a constant mini slump value of 150 mm. The nomenclature of each mixture refers to the amount of SAP, EA, and SRA, respectively (e.g., 0.5SAP10EA2SRA denotes a cement paste mixture made with 0.5 wt % SAP, 10 wt% EA, and 2 wt% SRA). The "AW" in the mixtures' name correspond to additional water that did not implicate increasing the SP demand. The REF implies the reference mixture made without any shrinkage mitigating strategies. The OPC was replaced by EA. The SRA,

Table 1
Physical and chemical characteristics of cementitious materials.

Oxide/Parameter	OPC	EA
SiO_2 [wt%]	18.7	12.6
Al_2O_3 [wt%]	4.0	5.7
Fe_2O_3 [wt%]	3.6	1.9
CaO [wt%]	65.9	82.6
MgO [wt%]	1.7	0.1
SO_3 [wt%]	2.4	–
$CaCO_3$ [wt%]	3.3	–
$Na_2O_{eq.}$ [wt%]	0.97	0.90
LOI [wt%]	1.5	–
Blaine surface area [m^2/kg]	390	–
Density [g/cm^3]	3.14	3.12

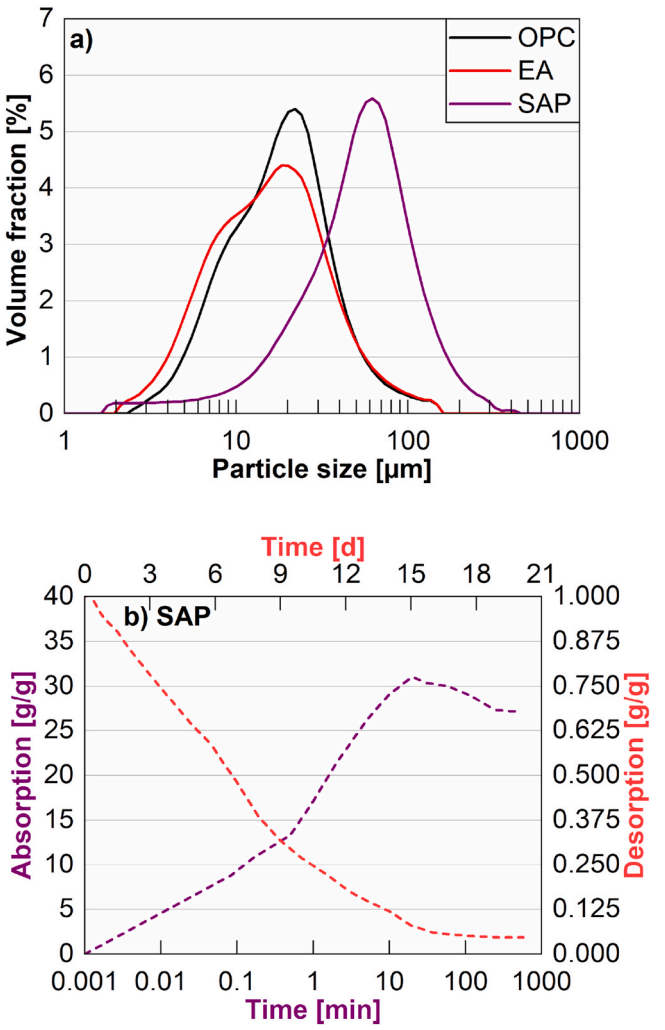

Fig. 1. (a) Particle size distribution of powder materials, (b) sorption curves for SAP.

Table 2
Characteristics of chemical admixtures.

Admixture	Solid content (wt%)	Specific gravity [−]
SP	23.0	1.05
SRA	30.0	1.10

Table 3
Mixture proportioning of investigated cement pastes.

Mixture	Absolute value [g/dm^3]						w/cm [−]
	OPC	EA	SRA	SAP	SP	Water	
REF	1,384	0	0	0	2.77	554	0.40
0.5SAP	1,384	0	0	6,92	8.30	554	0.40
0.5SAP10 EA	1,246	138	0	6.92	11.07	554	0.40
0.5SAP2SRA	1,384	0	27.68	6.92	8.30	554	0.40
0.5SAP + AW	1,384	0	0	6.92	2.77	758	0.55
0.5SAP10 EA + AW	1,246	138	0	6.92	2.77	758	0.55
0.5SAP2SRA + AW	1,384	0	27.68	6.92	2.77	739	0.55

SAP and SP were added by weight of cement.

2.3. Testing methods

2.3.1. Compressive strength and autogenous shrinkage

The cement paste (V = 5 L) was mixed in a large Hobart mixer according to ASTM C305-20 [49]. Cubic samples of 50 x 50 × 50 mm were cast for compressive strength testing. After casting, the molds were covered with a damp cloth to prevent the evaporation of free water. After 24 h, the cubes were demolded and stored in lime-saturated water at T = 23 ± 2 °C, until 7 days age. Then, the cubes were stored in the laboratory at an ambient temperature of 23 ± 2 °C. Compressive strength testing was conducted at 28 days according to ASTM C109-20 [50] using a Tinius Olsen universal testing machine with a loading rate of 0.89 kN/s and a break detection of 50%. The compressive strength values represent the average of at least three tested cubes.

Autogenous shrinkage was tested according to ASTM C1698-19 [51]. The cement pastes were filled in two lifts into corrugated polyethylene tubes and consolidated by rodding at least 10 times per lift. The tubes were sealed with caps to prevent any moisture loss and stored in the laboratory (T = 23 ± 2 °C). The length change was measured immediately after setting for 28 days with a digital comparator on at least two samples and the average values were reported.

2.3.2. Hydration kinetics

The heat flow [mW] of cement pastes was measured during the first 72 h of hydration with isothermal calorimeter Calmetrix I-Cal HPC 8000. The flow curves were recorded with the software CalCommander v.2.03. After mixing, the sample (m = 50 g) was transferred into a plastic cup that closed with a plastic lid. Temperature control was set at 20 °C. The measured heat flow was related to 1 g cement. The heat flow curves were interpreted according to the four stages of C_3S reaction in cement, as proposed by Bullard et al. [52]: I) initial formation, II) period of slow reaction (dormant period), III) acceleration period (up to the first maximum) and IV) deceleration period. Hesse et al. [53] associated a second heat maximum with a strong ettringite formation/C_3A dissolution, where the maximum ettringite content is reached and the formation of mono phases starts. The heat of hydration was obtained by the integration of the heat flow over time.

2.3.3. Sample preparation and microstructure analysis at 28 days

Cement paste pieces were extracted from the core of autogenous shrinkage samples at 28 days. Crushed samples' size ranged between 5 mm and 15 mm depending on the subsequent tests. Hydration of the samples was stopped using acetone. The acetone was removed via suction once the crushed paste was sedimented—a method adopted from Scherb et al. [54]. The samples were dried afterwards and stored in a small container under N_2 atmosphere until the respective measurement. Samples were manually ground for XRD and TG measurements to obtain particle sizes <63 μm.

2.3.4. X-Ray Diffraction (XRD)

XRD measurements were conducted with 30 wt% TiO_2 (ICSD file no. 01-078-2486) as internal standard to identify the crystalline phases of the hardened cement pastes. A Philips/Panalytical X'Pert Pro multipurpose diffractometer was used with a fixed divergence slit (DS = 0.38 mm), generator voltage of 45 kV and tube current of 40 mA with Cu Kα radiation. The measurement angle (2θ) ranged from 5 to 90°. The step size was 0.0263° and the time per step was 137.19 s. The qualitative phase composition was determined with X'Pert HighScore 5.1 and the Rietveld analysis with RIQAS. Relevant crystalline phases were ettringite (ICSD file no. 01-072-0646), portlandite (ICSD file no. 01-081-2040) and C_3S (ICSD file no. 01-086-0402).

2.3.5. Fourier-Transform Infrared Spectroscopy (FTIR)

Semi-quantitative phase analysis was conducted on ground cement paste by FTIR spectroscopy. The FTIR spectra were taken by a ThermoFisher Scientific Nicolet iS10 in attenuated total reflection. The FTIR spectrometer was equipped with a mid-infrared KBr beamsplitter, a diamond ATR crystal and a dTGS detector. The spectra range was 400–1000 cm^{-1} at a resolution of 4 cm^{-1}.

2.3.6. Thermogravimetric (TG) analysis

The TG method enabled the quantitative comparison of crystalline phases as identified with XRD, as well as the detection and quantification of further phases, such as X-ray amorphous C–S–H. Powder samples for TG measurements were dried in a climatic chamber at T = 50 °C (to prevent the decomposition of ettringite which starts between 60 and 74 °C [55]). Each sample (m = 250 mg) was inserted into an aluminum crucible and heated up at a rate of 2 K/min under air atmosphere in a Netzsch STA 449 F3 Jupiter. The respective mass loss/water release (H [g/g_{cement}]) was calculated in total 3 temperature intervals, as proposed by Beuntner and Thienel [56], based on Eq. (2). It considered the difference in mass between two temperatures ($\Delta m_{T1\text{-}T2}$), the cement proportion in the sample (f_c) and the weight of the sample (m_s).

$$H \text{ or } CO_2 = \frac{\Delta m_{T1-T2}}{f_c m_s} \bullet 100 \quad (2)$$

Further mass loss included the decomposition of the following hydrate phases:

- H_I (T = 20–140 °C): C–S–H and AFt [57].
- H_{IIa} (T = 140–320 °C): AFm phases (AFm-Hc, Mc, Ms [58]) and C_2AH_8 [59]
- H_{IIb} (T = 320–400 °C): AFm phases [60], C_3AH_6 and C_4AH_x [59]

The CH was decomposed between T = 450–530 °C [59], according to the Marsh & Day method [61], considering the dry sample mass at T = 400 °C as proposed by Beuntner [62].

2.3.7. Mercury Intrusion Porosity (MIP)

The volume and size distribution of accessible pores in hardened cement paste was determined by mercury intrusion porosimetry according to DIN 66133 [63]. After extraction, the samples (V = 1 cm^3) were stored for at least 3 days in isopropanol and subsequently dried at 70 °C. Afterwards, they cooled down to ambient temperature in a desiccator. The mercury intrusion porosimeter Pascal from Thermo Fisher Scientific consisting of a low-pressure unit (400 kPa) and of a high-pressure unit (400 MPa) corresponding to pore radii of 2 μm and 2 nm, respectively, was applied. For the calculation of porosity parameters, the contact angle (ϑ = 140°) and the surface tension (σ = 0.48 Nm) of mercury were inserted in the Washburn equation (Eq. (3)) [64], leading to the following relationship of pressure (p) to pore radius (r_p):

$$\frac{-2 \bullet \sigma}{p} r_p = \frac{-2 \bullet \sigma}{p} \cos 140 = 5.266 \bullet p \quad (3)$$

The pores were classified as gel pores (pore size diameter <30 nm), capillary pores (30 nm–50 μm), and air voids (>50 μm) [65].

2.3.8. Environmental Scanning Electron Microscopy (ESEM)

The morphology of freshly broken cement paste samples was investigated by environmental scanning electron microscopy (ESEM), using a Thermo Fisher Scientific Prisma ESEM in backscattered mode. In low vacuum, an aperture of and a gaseous secondary electron detector were used with acceleration voltage of 20 kV and working distance between 5.3 and 6.2 mm. ESEM complemented the previous methods by optical evaluation of the microstructure.

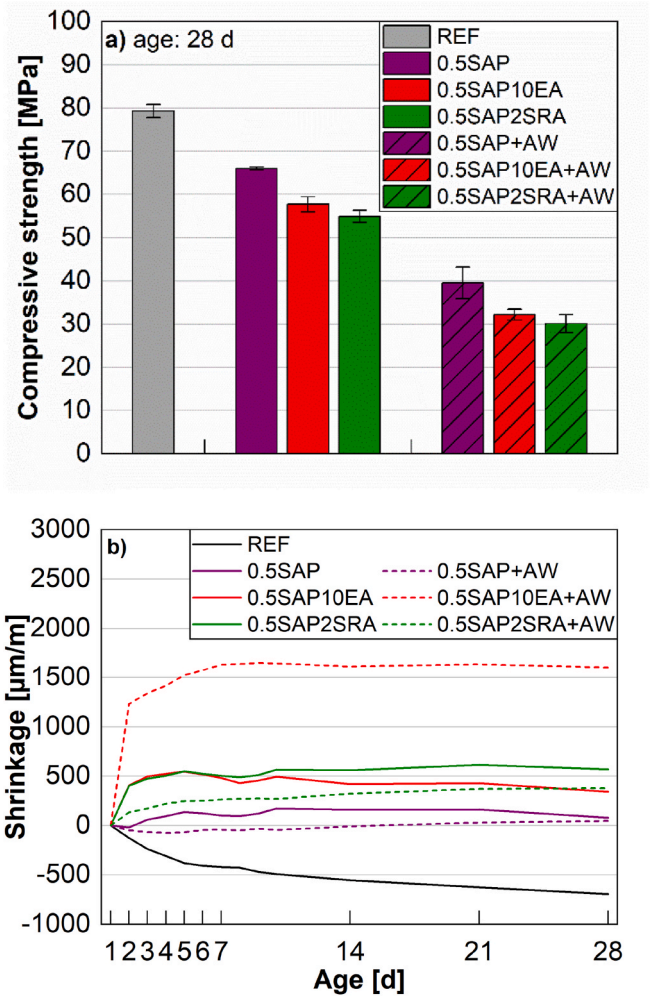

Fig. 2. (a) Compressive strength, (b) autogenous shrinkage of the investigated mixtures.

3. Results and discussion

3.1. Compressive strength and autogenous shrinkage

The compressive strength ranged between 30 and 79 MPa at 28 days (Fig. 2a). The highest strength was recorded for the REF mixture, while the lowest was recorded for 0.5SAP2SRA + AW mixture with additional water. The mixtures with 0.5 wt% SAP and without additional water exhibited up to 82% higher compressive strength compared to the mixtures with additional water. The additional water increased w/cm, and led to lower density and compressive strength as discussed in Ref. [46]. The addition of either EA or SRA coupled with SAP reduced the compressive strength compared to the 0.5SAP mixture. Up to 7% higher compressive strength was observed with the coupled use of SAP and EA compared to SAP and SRA. Further investigation on the mechanism of the effect of these materials is described in section 3.3.

Fig. 2b shows the evolution of autogenous shrinkage with time. The 28-day autogenous shrinkage at ranged between −700 µm/m for the REF mixture and 1600 µm/m (expansion) for the 0.5SAP10 EA mixture, the latter showing visible cracking. The rapid initial expansion due to the use of a high content of EA (10%) can be amplified in the presence of 0.5% SAP and additional water. The additional water can extend the hydration and formation of CH and lead to excessive expansion after 28 days. Although the combination of EA and SAP with additional water resulted in excessive expansion, the individual use of SAP and its combination with SRA led to a reasonable and higher expansion. The use of SRA in the presence of SAP induced higher expansion (350–500 µm/m more expansion) compared to the mixtures made with only SAP. The use of SRA in additional water mixture led to lower expansion than that of the corresponding mixture with additional SP. This will be justified by the higher heat of hydration associated with the latter mixture in section 3.2.

3.2. Hydration kinetics

The dormant period of individual and binary mixtures ranged between 1.2 and 2.5 h and varied significantly in the measured Q_{min} values, as shown in Fig. 3 and in Table 4. The 0.5SAP10 EA and 0.5SAP10 EA + AW mixtures exhibited higher Q_{min} values as the heat flow was related to 90 wt% of cement in binder. However, the respective Q_{min} value was up to 107% higher compared to REF mixture, which indicated an enhanced formation of hydrate phases within the first 2-3 h of hydration (Table 4). As consequence, the heat of hydration was 91% higher after 6 h already for 0.5SAP10 EA + AW mixture and both 0.5SAP10 EA mixtures exceeded the heat of hydration of REF mixtures beyond 12 h (Table 5). The compensation of SAP water absorption by entraining IC water extended the dormant period of 0.5SAP + AW and 0.5SAP10 EA + AW mixtures by 0.4 h compared to 0.5SAP and 0.5SAP10 EA mixtures, respectively. In both 0.5SAP2SRA mixtures, there was no difference between additional water or SP regarding the end of dormant period. Overall, the SP adjustment led to less retardation of the dormant period, but to a slight suppressed hydrate phase formation, as indicated by lower Q_{min} values.

As shown in Fig. 3 and Table 4, the highest and lowest cumulative heat of hydration after 72 h were associated with the 0.5SAP10 EA + AW (+28% compared to REF) and 0.5SAP (−9% compared to REF) with additional water and additional SP, respectively. The high hydration rate for the 0.5SAP10 EA + AW mixture attributed to the reaction of additional water and EA.

As discussed in section 3.1, this mixture exhibited the highest expansion. The use of additional SP instead of additional water delayed dormant period; however, this led to greater hydration peaks. The former mixtures presented higher initial expansion compared to the mixtures with additional water, except for the 0.5SAP10 EA mixture. The significantly higher peak of the 0.5SAP2SRA mixtures incorporating additional SP compared to the corresponding mixture with additional water confirms the high reaction and autogenous expansion of the former mixture (see section 3.1). Regarding the descending part of the curves, the mixtures incorporating SAP with additional water presented milder slope, which confirms their lower shrinkage rate after initial expansion (see section 3.1). Most of the mixtures showed a clearly

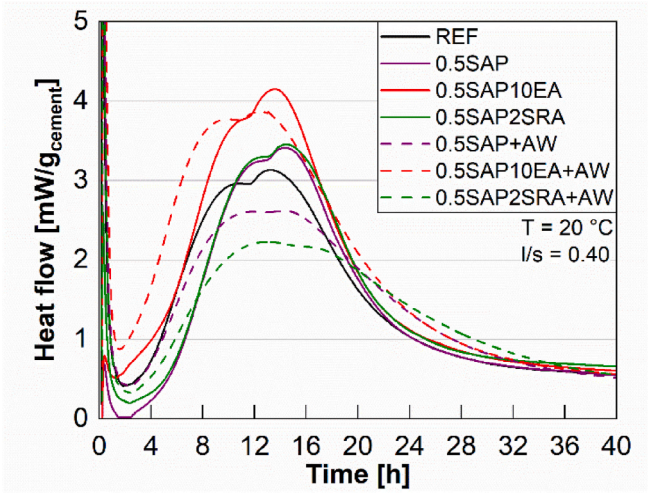

Fig. 3. Heat flow curves of the investigated cement paste mixtures.

Table 4
Significant values during heat flow measurements (Q_{min} = heat at end of dormant period, $t_{Q,min}$ = time of end of dormant period, $Q_{max,1/2}$ = heat maxima, $t_{Q,max,1/2}$ = time of heat maxima).

Mixture	Dormant period		Heat maxima			
	Q_{min} [mW/g_{cement}]	$t_{Q,min}$ [h]	$Q_{max,1}$ [mW/g_{cement}]	$t_{Q,max,1}$ [h]	$Q_{max,2}$ [mW/g_{cement}]	$t_{Q,max,2}$ [h]
REF	0.42	2.1	2.9	10.6	3.1	13.2
0.5SAP	0.01	2.0	3.2	12.1	3.4	14.4
0.5SAP10 EA	0.51	1.2	3.8	11.1	4.1	13.7
0.5SAP2SRA	0.19	2.4	3.3	12.3	3.4	14.5
0.5SAP + AW	0.40	2.4	2.6	11.4	2.6	14.7
0.5SAP10 EA + AW	0.87	1.6	3.8	9.5	3.9	12.6
0.5SAP2SRA + AW	0.32	2.5	2.2	12.6	2.1	17.2

Table 5
Heat of hydration at specific times up to 72 h.

Mixture	Heat of hydration [J/g_{cement}] after elapsed time [h]				
	6	12	24	48	72
REF	22	79	172	227	259
0.5SAP	5	52	154	209	236
0.5SAP10 EA	18	85	199	260	296
0.5SAP2SRA	10	58	164	226	260
0.5SAP + AW	21	70	162	221	255
0.5SAP10 EA + AW	42	119	234	295	332
0.5SAP2SRA + AW	18	56	141	205	237

visible, second peak that is associated with a strong ettringite formation and conversion of ettringite to monophases [53,66].

3.3. Hydrate phase composition and microstructural properties

3.3.1. X-ray diffraction and semi-quantitative analysis

Fig. 4 shows the XRD patterns of the investigated mixtures. Crystalline phases such as ettringite, portlandite (CH), and unhydrated C_3S/C_2S were detected. The CH was detected at 2θ of 18°, 34°, 47°, and 55.5°. The peaks associated with ettringite were mostly found at 2θ of 8° and 25.5°. The unhydrated C_3S/C_2S peaked at 2θ of 29.3°, 39°, and 51.6°. Except for the mixtures containing SRA, the higher intensity of the peaks associated with the mixtures including SAP and additional water compared to those made with additional SP confirms the higher extent of hydration in the former mixtures.

Table 6 summarizes the semi-quantitative analysis of the crystalline phases of the investigated cement paste mixtures at 28 days. The results show that except for the 0.5SAP2SRA mixture with additional SP, the use of SAP increased the rate of ettringite and CH phases compared to the REF mixture. The adverse effect of SRA on hydration due the reduction in the alkalinity of pore solution was reported in previous studies [15,32,67,68]. The highest content of ettringite was obtained by the 0.5SAP10 EA mixture with additional SP, which was 51% greater than that of the REF mixture. The highest CH content was recorded for the same mixture with additional water, which was 68% greater than the REF mixture. This high content of CH caused excessive autogenous expansion as observed in section 3.1.

Except for the 0.5SAP2SRA mixture, more ettringite was formed in the mixtures made with SAP and additional SP. The 0.5SAP and 0.5SAP10 EA mixtures made with SAP and additional SP obtained up to 35% higher ettringite compared to the counterpart mixtures made with additional water. The mixtures made with additional water recorded higher amounts of CH (up to 66%) compared to the counterpart mixtures made with additional SP. The mixtures made with additional SP included significantly higher unhydrated phases compared to the

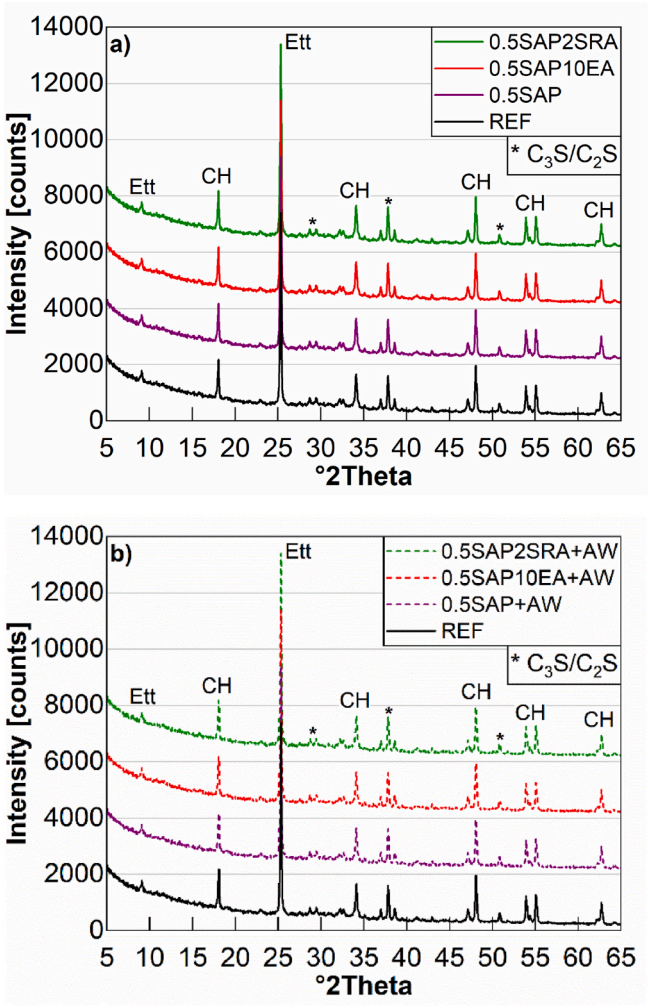

Fig. 4. XRD patterns of REF and for (a) mixtures made with SAP and additional SP, (b) mixtures made with SAP and additional water.

Table 6
Semi-quantitative analysis of ettringite, portlandite and unreacted phases of cement paste at 28 days.

Mixture	Ettringite [wt%]	Portlandite [wt%]	C_3S/C_2S [wt%]
REF	4.1	14.8	6.4
0.5SAP	4.2	16.6	8.2
0.5SAP10 EA	6.2	17.1	6.4
0.5SAP2SRA	3.7	13.9	7.5
0.5SAP + AW	4.1	20.3	3.3
0.5SAP10 EA + AW	4.6	24.9	4.4
0.5SAP2SRA + AW	4.7	23.1	4.5

counterpart mixtures made with additional water. This difference was up to 150%. These mixtures also were contained up to 30% higher unhydrated phases compared to the REF mixture. As expected, the high amount of unhydrated phases was due to the lack of water for hydration. However, since the additional water caused excessive expansion of SAP particles which created porosity into the matrix after SAP's water desorption, the corresponding mixtures exhibited inferior mechanical properties [46,69–72] [6,8,9,10,11].

3.3.2. Fourier-transform infrared spectroscopy

The FTIR transmission curves over wavenumber of selected mixtures are shown in Fig. 5. The portlandite specific O–H band visible at 3641 cm^{-1} [73] showed no significant differences in the intensity. Only the

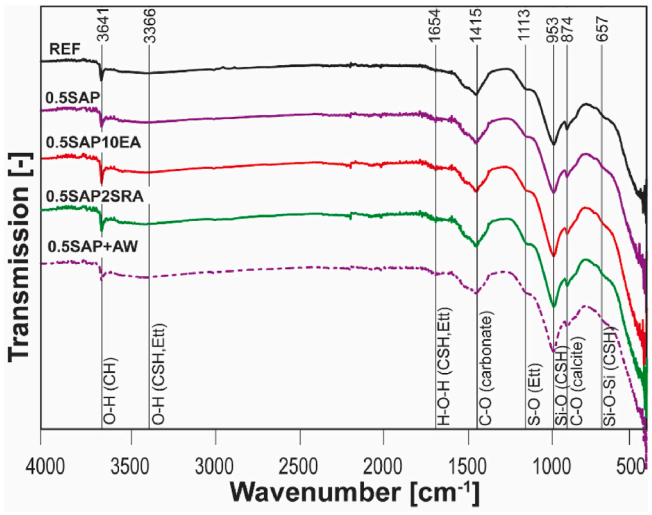

Fig. 5. FTIR graphs of selected cement pastes at 28 days.

0.5SAP10 EA mixture exhibited a greater intensity in portlandite band compared to the REF mixture. The bands associated with CSH and ettringite, at 3366 cm^{-1} (O–H) and 1654 cm^{-1} (H–O–H), exhibited weak humps with negligible intensity. The formation of CSH, which mainly is identified by Si–O band at 953 cm^{-1} [74], was higher for 0.5SAP + AW mixture compared to REF mixture, which indicated a stronger CSH formation due to the addition of water also compared to 0.5SAP. The 0.5SAP10 EA and 0.5SAP2SRA mixtures had higher and lower intensity of Si–O band compared to the REF mixture, respectively. This indicated that the synergetic effect of 10 wt% EA und 0.5 wt% SAP could enhance the formation of CSH, while the combination of 2 wt% SRA and 0.5 wt% SAP had a negligible effect on the formation of strength-building CSH. The formation of ettringite, identified by the S–O band at 1113 cm^{-1}, showed a greater intensity for both 0.5SAP mixtures, especially the one made with additional water. Based on the C–O bands at 1415 cm^{-1} and 657 cm^{-1} [75], the sensitivity to carbonation was slightly higher for the 0.5SAP + AW mixture (Fig. 5). These findings due to their limitation and comparative analysis of the peak shapes and intensities required to be verified by thermogravimetric analysis in the following section 3.3.3.

3.3.3. *Thermogravimetry*

All mixtures showed mass losses at the same temperature windows (Fig. 6). The first peak occurred at 110–140 °C, which is commonly attributed to the loss of chemically bound water in C–S–H and ettringite [59]. It was followed by a second peak at T = 150 - 170 °C that was related to carboaluminates (AFm-Hc, AFm-Mc) [58]. A small mass loss was recorded between 320 and 400 °C, that was related to C_3AH_6 [76] and traces of brucite ($Mg(OH)_2$) [77] formed from the MgO in cement (Table 1). The most significant mass loss was observed between 450 and 530 °C, where CH decomposes. The amount of bound water at respective temperature ranges and the mass of CH, as calculated by Marsh & Day, are provided in Table 7. Beyond this temperature, two more peaks were observed which were associated with the decarbonation of crystalline $CaCO_3$, between T = 530 and 1000 °C.

All mixtures made with shrinkage mitigating materials had a higher amount of bound water between 20 and 140 °C (H_I) than the REF mixture (Fig. 6 and Table 7). The highest H_I values were observed for those mixtures with 0.5 wt% SAP and additional water, namely 0.5SAP + AW, 0.5SAP10 EA + AW and 0.5SAP2SRA (4.1–5.6 wt%). Although the quantification according to Rietveld analysis in the previous section showed otherwise, it was considered that these mixtures contained more water available for the formation of water-rich ettringite crystals ($Ca_6Al_2(SO_4)_3(OH)_{12}{\cdot}26H_2O$ [78]) and C–S–H. The formation of carboaluminates (indicated as H_{IIa}) was less pronounced for mixtures with

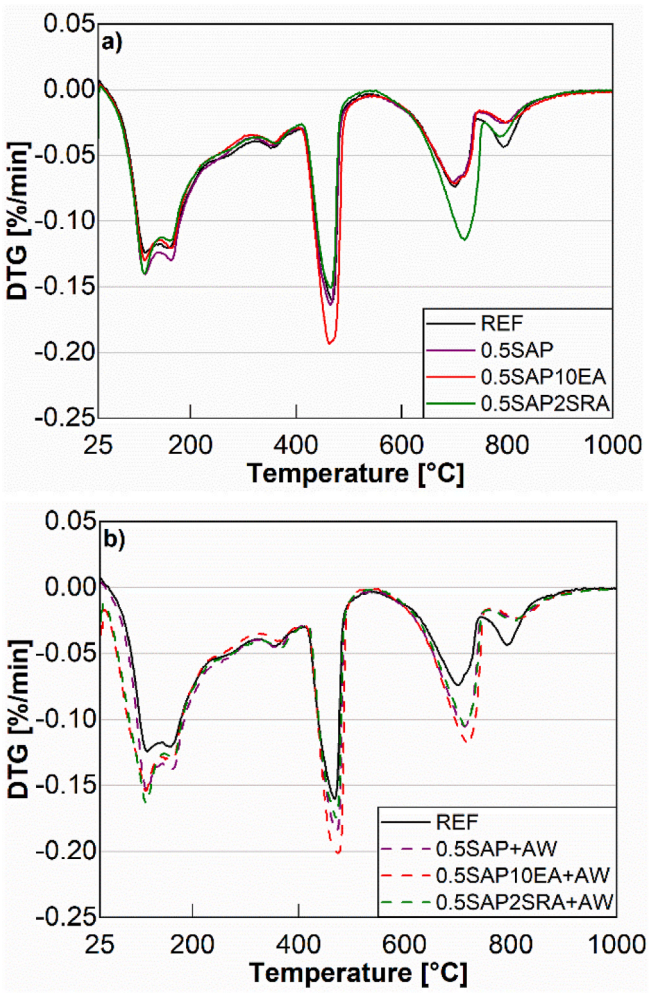

Fig. 6. DTG curves of investigated cement pastes (a) with adjusted dosage of SP, (b) with additional water compared to the REF mixture.

Table 7
Amount of bound water for temperature ranges up to 400 °C (H_I at T = 25–140 °C, H_{IIa} at T = 140–320 °C and H_{IIb} at T = 320–400 °C), release of CO_2 between 530 and 1000 °C, and CH content of hardened cement paste mixtures at 28 days.

Mixture	H_I [wt %]	H_{IIa} [wt %]	H_{IIb} [wt %]	CH [wt %]	CO_2 [wt %]
REF	3.4	6.2	1.7	7.2	5.1
0.5SAP	3.7	6.3	1.7	7.7	4.6
0.5SAP10 EA	3.5	5.9	1.5	9.4	4.7
0.5SAP2SRA	3.8	5.9	1.4	6.5	6.3
0.5SAP + AW	4.1	6.9	1.7	8.2	6.0
0.5SAP10 EA + AW	5.1	6.6	1.5	9.6	6.5
0.5SAP2SRA + AW	5.6	6.5	1.5	7.7	5.8

2 wt% SRA (respective amount of released water ≤6 wt%). Thus, the SRA slightly inhibited the formation of these hydrate phases. In 0.5SAP10 EA mixtures, though, the H_{IIa} values were increased by up to 11% compared to the REF mixture (6.2 wt%). Regarding the H_{IIb} values, the amount of C_3AH_6, the absolute difference was negligible with values between 1.4 wt% (for the 0.5SAP2SRA mixture) and 1.7 wt% (for the REF, 0.5SAP and 0.5SAP + AW mixtures). The portlandite formation, according to Marsh & Day theory, was more pronounced for mixtures with 10 wt% EA and 0.5 wt% SAP as observed via XRD (Table 6). This

confirmed at the one hand the enhanced formation of portlandite in the presence of CaO-based EA [13]. Higher available water content in mixtures with additional water led to higher portlandite formation as observed for 0.5SAP + AW and 0.5SAP2SRA + AW compared to 0.5SAP and 0.5SAP2SRA, respectively. The addition of 2 wt% SRA reduced the formation of hydrated phases, thus lower portlandite as indicated by lower amounts of bound water was found. This effect was especially prominent for the 0.5SAP2SRA mixture.

The degree of carbonation, ranged from 4.6 wt% CO_2 for the 0.5SAP mixture to 6.5 wt% CO_2 for the 0.5SAP10 EA + AW mixture. Compared to the REF mixture, most mixtures released up to 27% more CO_2 indicating a higher sensitivity to carbonation despite the identical curing for all the samples. This was related to the higher porosity of the mixtures, which will be discussed in section 3.3.44.

3.3.4. Mercury intrusion porosimetry (MIP)

The median pore size was in the range of 27 nm for the 0.5SAP2SRA mixture to 53 nm for the 0.5SAP2SRA + AW mixture (Table 8). The total capillary porosity was the lowest for the REF mixture (19.4%) and highest for the 0.5SAP10 EA + AW mixture. In general, those mixtures containing 0.5 wt% SAP and additional water (0.5SAP + AW, 0.5SAP10 EA + AW and 0.5SAP2SRA + AW mixtures) presented higher total porosity of 19%, 48% and 38% compared to 0.5SAP, 0.5SAP10 EA and 0.5SAP2SRA, respectively. This confirmed that increasing the effective w/cm leads to higher porosity [79], which significantly reduced the compressive strength, as discussed in section 3.1, and the correlation in Fig. 7 demonstrates. Thus, the adjustment of SP dosage instead of additional water is crucial to limit the porosity and loss of compressive strength. Mechtcherine et al. [69] showed that the porosity induced by SAP voids is highly dependent on the amount of used water and can significantly affect the compressive strength.

However, it is crucial to differentiate between the different types of pores and not only consider the total porosity. According to Table 8, limited (≤0.4%) large pores were exist in the 0.5SAP, 0.5SAP + AW and 0.5SAP2SRA mixtures. The capillary pores, that are responsible for the transport of damaging SO_3^-, Cl^- and CO_2 [80,81], represented 59% of all pores in the REF mixture. This percentage was increased for 0.5SAP + AW and 0.5SAP2SRA + AW mixtures, which indicated in combination with a higher total porosity an increased sensitivity towards capillary suction. The 0.5SAP10 EA and 0.5SAP2SRA mixtures showed a significant shift from capillary pores to gel pores. Their increased porosity compared to the REF mixture and reduction in the capillary pores can be beneficial and improve the durability of these mixtures. The pore size refinement resulting from modified hydration is a common phenomenon observed in other cementitious mixtures, such as calcined clay blends [65,82]. In addition, the adequate swelling of SAP particles leads to a higher gel porosity and overall denser microstructure in the aforementioned mixtures as long as the SP dosage is adjusted.

Table 8
Porosity parameters of hardened cement paste at 28 days.

Mixture	Median pore size [nm]	Total porosity [%]	Percentage of pore type on total pore volume [%]		
			Gel pores (d < 30 nm)	Capillary pores 30 nm < d < 50 μm)	Air voids (d > 50 μm)
REF	38	19.4	41.0	59.0	0.0
0.5SAP	31	24.9	47.0	52.6	0.4
0.5SAP10 EA	29	24.8	53.2	46.8	0.0
0.5SAP2SRA	27	24.4	69.0	30.8	0.2
0.5SAP + AW	43	29.7	41.1	58.7	0.2
0.5SAP10 EA + AW	48	36.8	41.4	58.6	0.0
0.5SAP2SRA + AW	53	33.8	36.5	63.5	0.0

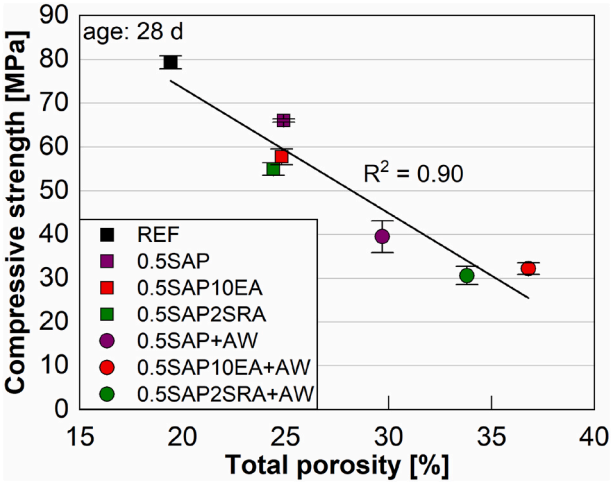

Fig. 7. Correlation of total porosity and compressive strength values of the investigated mixtures at 28 days.

3.3.5. Environmental scanning electron microscopy

The ESEM images for the REF mixture and mixtures incorporating 0.5 wt% SAP and additional water are shown in Fig. 8. The REF mixture showed a dense matrix at a magnification of 1000x, without cracking nor needle-like hydrate phases (Fig. 8a). Compared to this, the 0.5SAP mixture exhibited a more porous structure (Fig. 8b) confirming the higher porosity as measured by MIP in Section 3.3.4. In addition, the presence of ettringite needles provided information about a higher percentage of ettringite in 0.5SAP + AW compared to REF mixture, as higher magnification images (shown in Appendix) revealed. This correlated with the higher amount of bound water H_I from thermal analysis (Table 7) despite the same percentual amount of ettringite found by Rietveld analysis (that is because the amorphous content in XRD analysis is not detected). The 0.5SAP10 EA + AW and 0.5SAP2SRA + AW mixtures both showed a carpet of ettringite needles. Similar to the 0.5SAP + AW mixture, this was related to the increased amount of H_I in mixtures made with additional water compared to the REF mixture. The large amount of additional water enabled here the formation of more ettringite crystals, confirming the hypothesis from thermogravimetric analysis findings in Section 3.3.3.

4. Conclusions

The effect of additional water or SP on the performance of cement paste incorporating a relatively high content of 0.5 wt% SAP coupled with 10 wt% EA or 2 wt% SRA was investigated.

Compressive strength, autogenous shrinkage, and advanced material characterization techniques such as XRD, TG, MIP, FTIR, and SEM were employed to shed the light on the uncertainty about the use of SAP with additional water or SP coupled with EA or SRA. Based on the findings, the following conclusions can be drawn:

- The highest compressive strength and lowest porosity were both obtained for the REF mixture. The compressive strength of the mixtures made with additional SP were up to 80% higher than the mixtures with additional water.
- The mixtures made with SAP with additional SP exhibited up to 33% and 96% lower porosity and median pore size distribution, respectively, compared to the mixtures made with additional water.
- The use of SAP with SP adjustment was more effective in mitigating autogenous shrinkage compared to the use of additional water. The use of SAP coupled with EA without additional water significantly reduced the excessive autogenous expansion by less portlandite formation.

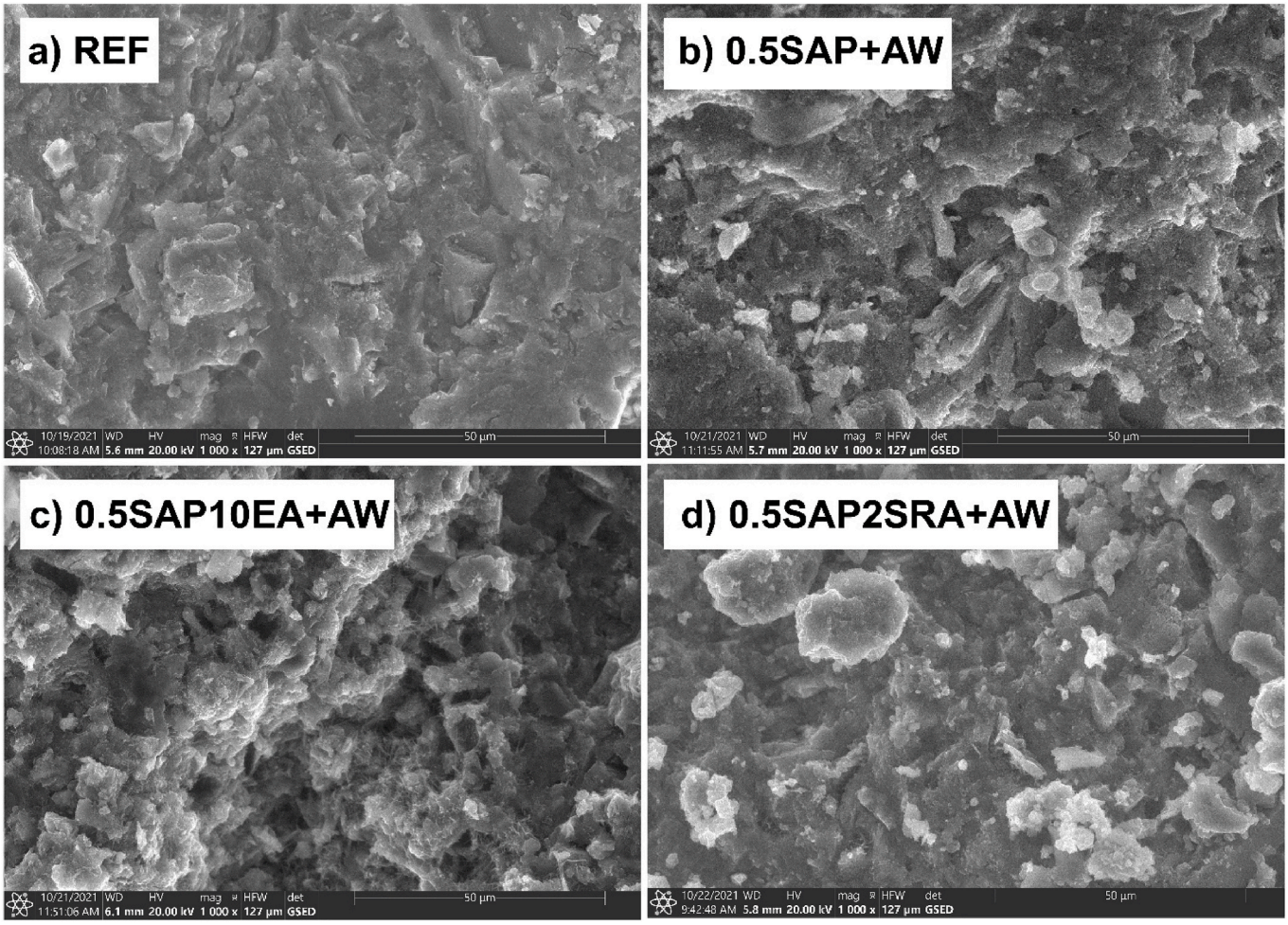

Fig. 8. SEM images of (a) REF, (b) 0.5SAP, (c) 0.5SAP10 EA + AW, and (d) 0.5SAP2SRA + AW at 28 days (magnification 1000x).

- FTIR analysis revealed an enhanced formation of CH and CSH in the 0.5SAP10 EA + AW mixture, induced by the addition of 10 wt% CaO-based EA. Contrary to this, the CH bands in the 0.5SAP2SRA were minor. The additional water led to a higher amount of ettringite formation, which was confirmed by comparing ESEM images of the 0.5SAP + AW, 0.5SAP10 EA + AW and 0.5SAP2SRA + AW mixtures.
- TG analysis showed that the use of SAP with additional water promoted CH formation by 18% compared to the counterpart mixtures made with additional SP.
- The cumulative heat of hydration at 72h was 10% higher for mixtures made with SAP and additional water compared to those with additional SP, except for the 0.5SAP2SRA mixture. A lower cumulative heat of hydration was attributed to the effect of higher water content coupled with SRA that reduces surface tension of capillary pores and alkalinity of the pore solution, and delays hydration reaction.
- The results showed that using an extra 0.6% SP instead of 30 g/g of SAP additional water in cement paste containing high content of SAP can improve the mechanical properties, shrinkage, and microstructure. These findings can allow the use of high content of SAP in combination with other shrinkage mitigating materials in high performance cement composites without compromising the performance.

Declaration of competing interest

The authors declare that they have no known competing financial interests or personal relationships that could have appeared to influence the work reported in this paper.

Data availability

Data will be made available on request.

Acknowledgement

The authors would like to thank Dr. Mathias Köberl from the Institute for Construction Materials at the University of the Bundeswehr Munich, Germany, for conducting the measurements and analysis of FTIR, TG, and MIP experiments.

Appendix A. Higher magnification SEM images

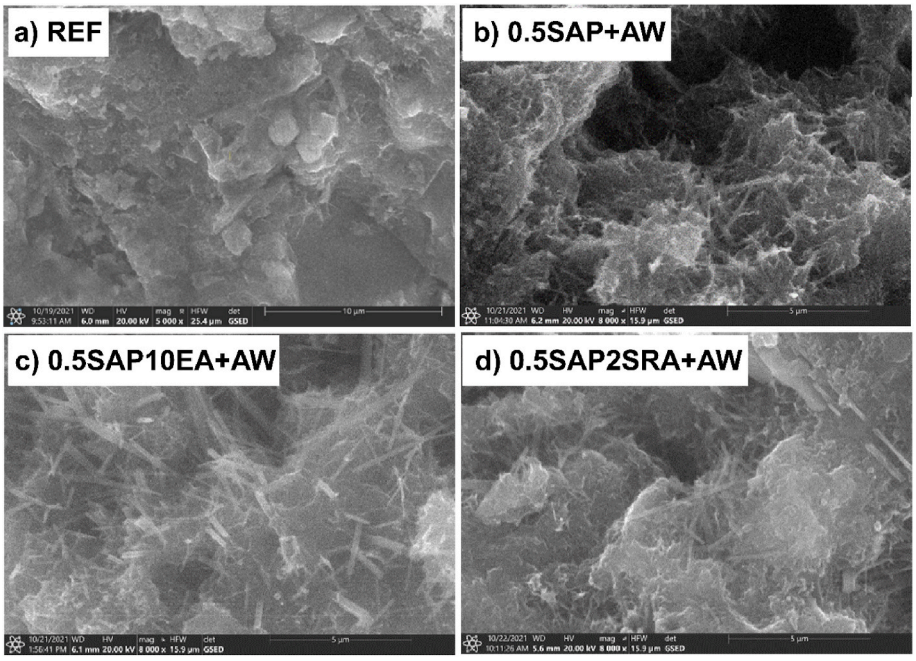

Fig. A1. SEM images of a) REF (magnification 5k), b) 0.5SAP (magnification 8k), c) 0.5SAP10 EA + AW (magnification 8k), and d) 0.5SAP2SRA + AW (magnification 8k) at 28 days

References

[1] A. Bentur, S.-i. Igarashi, K. Kovler, Prevention of autogenous shrinkage in high-strength concrete by internal curing using wet lightweight aggregates, Cement Concr. Res. 31 (11) (2001) 1587–1591.

[2] M.H.N. Yio, et al., Effect of autogenous shrinkage on microcracking and mass transport properties of concrete containing supplementary cementitious materials, Cement Concr. Res. 150 (2021), 106611.

[3] P.-C. Aitcin, A.M. Neville, P. Acker, Integrated view of shrinkage deformation, Concr. Int. 19 (9) (1997) 35–41.

[4] K. Aghaee, K.H. Khayat, Effect of shrinkage-mitigating materials on performance of fiber-reinforced concrete – an overview, Construct. Build. Mater. 305 (2021), 124586.

[5] K. Aghaee, N. Farzadnia, K.H. Khayat, Coupled effect of expansive agent and curing on mechanical and shrinkage properties of fiber-reinforced Eco-Crete, Construct. Build. Mater. 310 (2021), 125285.

[6] P. Zhong, et al., Internal curing with superabsorbent polymers of different chemical structures, Cement Concr. Res. 123 (2019), 105789.

[7] P. Yan, X. Qin, The effect of expansive agent and possibility of delayed ettringite formation in shrinkage-compensating massive concrete, Cement Concr. Res. 31 (2) (2001) 335–337.

[8] L. Yang, C. Shi, Z. Wu, Mitigation techniques for autogenous shrinkage of ultra-high-performance concrete – a review, Compos. B Eng. 178 (2019), 107456.

[9] P.K. Mehta, Mechanism of expansion associated with ettringite formation, Cement Concr. Res. 3 (1) (1973) 1–6.

[10] V. Corinaldesi, A. Nardinocchi, J. Donnini, The influence of expansive agent on the performance of fibre reinforced cement-based composites, Construct. Build. Mater. 91 (2015) 171–179.

[11] Z.-h. Feng, Influence of temperature on the hydration heat evolution of shrinkage-compensating complex binders, J. Chin. Ceram. Soc. 34 (8) (2006) 1006–1010.

[12] H. Zhao, et al., Effects of curing temperature and superabsorbent polymers on hydration of early-age cement paste containing a CaO-based expansive additive, Mater. Struct. 52 (6) (2019) 108.

[13] Y. Wang, et al., Humidity sensitivity of hydration of expansive agent and its expansive efficiency in ultra-high performance concrete, Crystals 12 (2) (2022) 195.

[14] G. Gelardi, et al., Chemistry of chemical admixtures, in: P.-C. Aïtcin, R.J. Flatt (Eds.), Science and Technology of Concrete Admixtures, Woodhead Publishing, 2016, pp. 149–218.

[15] F. Rajabipour, G. Sant, J. Weiss, Interactions between shrinkage reducing admixtures (SRA) and cement paste's pore solution, Cement Concr. Res. 38 (5) (2008) 606–615.

[16] S. Gao, et al., Effect of shrinkage-reducing admixture and expansive agent on mechanical properties and drying shrinkage of Engineered Cementitious Composite (ECC), Construct. Build. Mater. 179 (2018) 172–185.

[17] J.-Y. Wang, N. Banthia, M.-H. Zhang, Effect of shrinkage reducing admixture on flexural behaviors of fiber reinforced cementitious composites, Cement Concr. Compos. 34 (4) (2012) 443–450.

[18] J.-J. Park, et al., Benefits of using expansive and shrinkage-reducing agents in UHPC for volume stability, Mag. Concr. Res. 66 (14) (2014) 745–750.

[19] A.M. Soliman, M.L. Nehdi, Effects of shrinkage reducing admixture and wollastonite microfiber on early-age behavior of ultra-high performance concrete, Cement Concr. Compos. 46 (2014) 81–89.

[20] D.-Y. Yoo, et al., Effect of shrinkage-reducing admixture on biaxial flexural behavior of ultra-high-performance fiber-reinforced concrete, Construct. Build. Mater. 89 (2015) 67–75.

[21] A.N.M. Lopes, et al., Shrinkage-reducing admixture: effects on durability of high-strength concrete, ACI Mater. J. 110 (4) (2013) 365–374.

[22] V. Mechtcherine, E. Secrieru, C. Schröfl, Effect of superabsorbent polymers (SAPs) on rheological properties of fresh cement-based mortars — development of yield stress and plastic viscosity over time, Cement Concr. Res. 67 (2015) 52–65.

[23] X.-m. Kong, Z.-l. Zhang, Z.-c. Lu, Effect of pre-soaked superabsorbent polymer on shrinkage of high-strength concrete, Mater. Struct. 48 (9) (2015) 2741–2758.

[24] V. Mechtcherine, et al., Effect of internal curing by using superabsorbent polymers (SAP) on autogenous shrinkage and other properties of a high-performance fine-grained concrete: results of a RILEM round-robin test, Mater. Struct. 47 (3) (2014) 541–562.

[25] M. Wyrzykowski, et al., Recommendation of RILEM TC 260-RSC: using superabsorbent polymers (SAP) to mitigate autogenous shrinkage, Mater. Struct. 51 (5) (2018) 135.

[26] C. Schröfl, et al., Recent progress in superabsorbent polymers for concrete, Cement Concr. Res. 151 (2022), 106648.

[27] L. Senff, et al., Development of mortars containing superabsorbent polymer, Construct. Build. Mater. 95 (2015) 575–584.

[28] K. Farzanian, A. Ghahremaninezhad, Desorption of superabsorbent hydrogels with varied chemical compositions in cementitious materials, Mater. Struct. 51 (1) (2018) 3.

[29] J. Liu, et al., Effects of SAP characteristics on internal curing of UHPC matrix, Construct. Build. Mater. 280 (2021), 122530.

[30] L. De Meyst, et al., The influence of superabsorbent polymers (SAPs) on autogenous shrinkage in cement paste, mortar and concrete, Construct. Build. Mater. 286 (2021), 122948.

[31] O.M.J. Jensen, P.F. Hansen, Water-entrained cement-based materials I. Princples and theoretical background, Cement Concr. Res. 31 (4) (2001) 647–654.

[32] Y. Wehbe, A. Ghahremaninezhad, Combined effect of shrinkage reducing admixtures (SRA) and superabsorbent polymers (SAP) on the autogenous shrinkage, hydration and properties of cementitious materials, Construct. Build. Mater. 138 (2017) 151–162.

[33] J. Justs, et al., Influence of superabsorbent polymers on hydration of cement pastes with low water-to-binder ratio, J. Therm. Anal. Calorim. 115 (1) (2014) 425–432.

[34] L.P. Esteves, I. Lukošiūtė, J. Čėsnienė, Hydration of cement with superabsorbent polymers, J. Therm. Anal. Calorim. 118 (2) (2014) 1385–1393.
[35] J. Justs, et al., Internal curing by superabsorbent polymers in ultra-high performance concrete, Cement Concr. Res. 76 (2015) 82–90.
[36] Z. Li, et al., Internal curing by superabsorbent polymers in alkali-activated slag, Cement Concr. Res. 135 (2020), 106123.
[37] Q. Zhu, C.W. Barney, K.A. Erk, Effect of ionic crosslinking on the swelling and mechanical response of model superabsorbent polymer hydrogels for internally cured concrete, Mater. Struct. 48 (7) (2015) 2261–2276.
[38] O.M.J. Jensen, P.F. Hansen, Water-entrained cement-based materials II. Experimental observations, Cement Concr. Res. 32 (6) (2002) 973–978.
[39] D. Snoeck, L. Pel, N. De Belie, Comparison of different techniques to study the nanostructure and the microstructure of cementitious materials with and without superabsorbent polymers, Construct. Build. Mater. 223 (2019) 244–253.
[40] B. Craeye, M. Geirnaert, G.D. Schutter, Super absorbing polymers as an internal curing agent for mitigation of early-age cracking of high-performance concrete bridge decks, Construct. Build. Mater. 25 (1) (2011) 1–13.
[41] F.C.R. Almeida, A.J. Klemm, Efficiency of internal curing by superabsorbent polymers (SAP) in PC-GGBS mortars, Cement Concr. Compos. 88 (2018) 41–51.
[42] M.T. Hasholt, et al., Can superabsorent polymers mitigate autogenous shrinkage of internally cured concrete without compromising the strength? Construct. Build. Mater. 31 (2012) 226–230.
[43] Z. Yu, et al., Investigation of SAP content on the shrinkage and tensile properties of ultra-high performance concrete, Construct. Build. Mater. 345 (2022), 128402.
[44] M. Geiker, D.P. Bentz, O.M. Jensen, Mitigating Autogenous Shrinkage by Internal Curing, vol. 218, ACI Symposium Publication, 2004, pp. 143–154.
[45] M. Valipour, K.H. Khayat, Coupled effect of shrinkage-mitigating admixtures and saturated lightweight sand on shrinkage of UHPC for overlay applications, Construct. Build. Mater. 184 (2018) 320–329.
[46] K. Aghaee, R. Sposito, K.H. Khayat, Synergetic effect of shrinkage mitigating materials on rheological properties of flowable and thixotropic cement paste for 3D printing, Cement Concr. Compos. 133 (2022) 104686.
[47] C.J. Adams, et al., Evaluation of mix design strategies to optimize flow and strength of mortar internally cured with superabsorbent polymers, Construct. Build. Mater. 324 (2022), 126664.
[48] K. Aghaee, K.H. Khayat, Benefits and drawbacks of using multiple shrinkage mitigating strategies on performance of fiber-reinforced mortar, Cement Concr. Compos. 133 (2022), 104714.
[49] ASTM C305-20, *Standard Practice for Mechanical* Mixing of Hydraulic Cement Pastes and Mortars of Plastic Consistency, ASTM International, West Conshohocken, PA, USA, 2020, p. 3.
[50] ASTM C109/C109M-20, *Standard Test Method For Compressive Strength Of* Hydraulic Cement Mortars (Using 2-in. Or [50-mm] Cube Specimens), ASTM International, West Conshohocken, PA, 2020, p. 11.
[51] ASTM C1698 - 19, *Standard Test Method For Autogenous* Strain of Cement Paste and Mortar, ASTM International, West Conshohocken, PA, USA, 2019, p. 8.
[52] J.W. Bullard, et al., Mechanisms of cement hydration, Cement Concr. Res. 41 (12) (2011) 1208–1223.
[53] C. Hesse, F. Goetz-Neunhoeffer, J. Neubauer, A new approach in quantitative in-situ XRD of cement pastes: correlation of heat flow curves with early hydration reactions, Cement Concr. Res. 41 (1) (2011) 123–128.
[54] S. Scherb, et al., Quantitative X-ray diffraction of free, not chemically bound water with the PONKCS method, J. Appl. Crystallogr. 51 (6) (2018) 1535–1543.
[55] P.W. Brown, J.V. Bothe, The stability of ettringite, Adv. Cement Res. 5 (18) (1993) 47–63.
[56] N. Beuntner, K.-C. Thienel, Pozzolanic efficiency of calcined clays in blended cements with focus on the early hydration, Adv. Cement Res. 34 (8) (2022) 341–355.
[57] H.F.W. Taylor, Cement Chemistry, vol. 2, Thomas Telford Ltd, London, 1997, p. 459.
[58] B. Lothenbach, et al., Influence of limestone on the hydration of Portland cements, Cement Concr. Res. 38 (6) (2008) 848–860.
[59] V.S. Ramachandran, et al., Handbook of Thermal Analysis of Construction Materials, Elsevier Science, Norwich, NY, 2002.
[60] T. Matschei, B. Lothenbach, F.P. Glasser, Thermodynamic properties of Portland cement hydrates in the system CaO–Al2O3–SiO2–CaSO4–CaCO3–H2O, Cement Concr. Res. 37 (10) (2007) 1379–1410.
[61] B.K. Marsh, R.L. Day, Pozzolanic and cementitious reactions of fly ash in blended cement pastes, Cement Concr. Res. 18 (2) (1988) 301–310.
[62] N. Beuntner, Zur Eignung und Wirkungsweise calcinierter Tone als reaktive Bindemittelkomponente in Zement (On the suitability and mode of action of calcined clays as reactive binder components in cement), in: Deutscher Ausschuss für Stahlbeton, vol. 628, Beuth Verlag, Berlin, Germany, 2019, 207.
[63] DIN 66133, *Bestimmung der Porenvolumenverteilung und der spezifischen Oberfläche von Feststoffen durch Quecksilberintrusion (Determination of pore volume distribution and specific surface area of solids by mercury intrusion)*, Beuth Verlag, Berlin, Germany, 1993, p. 3.
[64] E.W. Washburn, The dynamics of capillary flow, Phys. Rev. 17 (3) (1921) 273–283.
[65] A. Tironi, et al., Influence of different calcined clays to the water transport performance of concretes, Mag. Concr. Res. 74 (14) (2022) 702–714.
[66] T. Matschei, B. Lothenbach, F.P. Glasser, The AFm phase in Portland cement, Cement Concr. Res. 37 (2) (2007) 118–130.
[67] V. Bílek, et al., Some issues of shrinkage-reducing admixtures application in alkali-activated slag systems, Materials 9 (6) (2016) 462.
[68] J. Saliba, et al., Influence of shrinkage-reducing admixtures on plastic and long-term shrinkage, Cement Concr. Compos. 33 (2) (2011) 209–217.
[69] V. Mechtcherine, et al., Application of super absorbent polymers (SAP) in concrete construction—update of RILEM state-of-the-art report, Mater. Struct. 54 (2) (2021) 80.
[70] A. Pourjavadi, et al., Improving the performance of cement-based composites containing superabsorbent polymers by utilization of nano-SiO2 particles, Mater. Des. 42 (2012) 94–101.
[71] G. Lefever, et al., Combined use of superabsorbent polymers and nanosilica for reduction of restrained shrinkage and strength compensation in cementitious mortars, Construct. Build. Mater. 251 (2020), 118966.
[72] S. Zhutovsky, K. Kovler, A. Bentur, Influence of cement paste matrix properties on the autogenous curing of high-performance concrete, Cement Concr. Compos. 26 (5) (2004) 499–507.
[73] M. Khachani, et al., *Non-isothermal kinetic and thermodynamic studies of the dehydroxylation process of synthetic calcium hydroxide* $Ca(OH)_2$, J. Mater. Environ. Sci. 5 (2) (2014) 615–624.
[74] A. Madadi, J. Wei, Characterization of calcium silicate hydrate gels with different calcium to silica ratios and polymer modifications, Gels 8 (2) (2022) 75.
[75] S. Steiner, et al., Effect of relative humidity on the carbonation rate of portlandite, calcium silicate hydrates and ettringite, Cement Concr. Res. 135 (2020), 106116.
[76] V.S. Ramachandran, Elucidation of the role of chemical admixtures in hydrating cements by DTA technique, Thermochim. Acta 4 (3) (1972) 343–366.
[77] I. Hager, Colour change in heated concrete, Fire Technol. 50 (4) (2014) 945–958.
[78] F. Goetz-Neunhoeffer, J. Neubauer, *Refined ettringite* $(Ca_6Al_2(SO_4)_3(OH)_{12}\bullet 26H_2O)$ *structure for quantitative X-ray diffraction analysis*, Powder Diffr. 21 (1) (2005) 4–11.
[79] A. Elsharief, M.D. Cohen, J. Olek, Influence of aggregate size, water cement ratio and age on the microstructure of the interfacial transition zone, Cement Concr. Res. 33 (11) (2003) 1837–1849.
[80] S. Sui, et al., Towards a generic approach to durability: factors affecting chloride transport in binary and ternary cementitious materials, Cement Concr. Res. 124 (2019), 105783.
[81] P. Barnes, J. Bensted, Structure and Performance of Cements, vol. 2, CRC Press, 2001, p. 584.
[82] J.M. Khatib, S. Wild, Pore size distribution of metakaolin paste, Cement Concr. Res. 26 (10) (1996) 1545–1553.